

Study report on
LCGT interferometer observation band

LCGT Special Working Group

September 8, 2009

Contents

1	Executive summary	3
2	Optical parameter candidates	7
2.1	Basic configuration and constraints	7
2.2	Broad band configuration	8
2.3	Detuned configuration	11
2.4	Variable tuning configuration	11
2.5	Summary of candidate parameter sets	11
3	Scientific outcomes from GW observation	13
3.1	Neutron star binary coalescences	13
3.2	Black-hole binary coalescences	14
3.3	BH quasi-normal mode	17
3.4	Supernovae with stellar-core collapse	17
3.5	Pulsar and LMXB	17
3.6	International Network of GW observation	19
4	Technical Feasibility	20
4.1	Interferometer control	20
4.2	Mirror loss	24
4.3	Calibration	24
5	Project strategy	25
5.1	Commissioning time	25
5.2	Cost comparison	25
5.3	Risks in noise hunting and diagnosis	25
5.4	Potential for future upgrades	25
A	Special Working Group members	26
B	Interferometer Sensing and Control Scheme	27
B.1	Sideband resonant conditions	27
B.2	Optickle simulation	29
B.2.1	Detuning range for signal recycling cavity	32
B.2.2	Selection of signal extraction ports	32
B.2.3	Loop coupling noise	33
B.2.4	Reduction of NS-NS binary range by loop coupling noise	34
C	Sub-carrier injection scheme	34

1 Executive summary

The purpose of this working group is to investigate and to make recommendations on the interferometer optical configuration design of LCGT and its observation band for gravitational waves. Advantages and disadvantages of candidate interferometer configurations have been surveyed from viewpoints of scientific possibilities, technical feasibilities, and project strategy. As a result, we recommend the following interferometer design and observation strategy.

Recommendations

- The optical configuration of LCGT should be VRSE: a RSE (resonant-sideband extraction) with variable observation band.
- In the first observation phase, LCGT interferometer should be operated with a detuned mode, VRSE (D), for earlier detection of gravitational-wave signals. After the first detections, the variable configuration provides the option to change the observation band to broadband, VRSE (B), so as to obtain more scientific information.

Candidate configurations

In the baseline design, LCGT has a RSE (Resonant Sideband Extraction) interferometer configuration. With this design, it is possible to optimize and tune the observation frequency band for target gravitational-wave sources, by choosing suitable optical parameters. So as to determine the optical parameters, we define three candidate parameter sets: broadband RSE (**BRSE**), detuned RSE (**DRSE**), and variable RSE (**VRSE**) configurations. In DRSE, the detector observation band is optimized by means of a detuning technique¹, to have maximum sensitivity for neutron-star inspiral events, which are the primary targets of LCGT. The parameters of BRSE are also optimized for these events, but with broadband (tuned) configuration. On the other hand, VRSE is designed to have good sensitivity both with tuned and detuned operation, and to switch observation bands depending on the observation purposes and targets².

The detector sensitivity curves are estimated with the current best-estimated boundary conditions of LCGT: an input laser power, suspension and mirror thermal noises, seismic noise, and optical readout noises. The estimated sensitivity curves are shown in Fig. 1. The DRSE configuration (green curve) has the best floor-level sensitivity at around 100 Hz, and the best observable distance of 132 Mpc for neutron-star inspiral events³. The BRSE configuration (red curve) has wider observation band to cover various sources, and moderate observable range of 114 Mpc for neutron-star inspirals. The blue and sky-blue curves are for the VRSE configuration with a detuned mode **VRSE (D)** and with a broadband mode **VRSE (B)**, respectively. They have slightly narrower and wider observation bands than the BRSE (red curve) configuration, respectively.

Comparisons between the candidates

Firstly, these candidate configurations are compared from a viewpoint of expected scientific outcomes (details are describes in Section 3). The purposes of LCGT are (1) to detect gravi-

¹Detuning is a technique to increase detector sensitivity only in a slightly narrow frequency band. It is realized by controlling the signal-extraction-cavity length between resonance and anti-resonance condition for the carrier laser beam.

²In this investigation, the VRSE configuration is designed so that the detuned/broadband modes would be switched with minimum observation dead times, without replacing or moving mirrors.

³Here, observable distance is defined as the range within which events are detected with higher signal-to-noise ratio than 8. Detector antenna pattern and wave polarizations are all-sky-averaged. Details are described in Section 3.

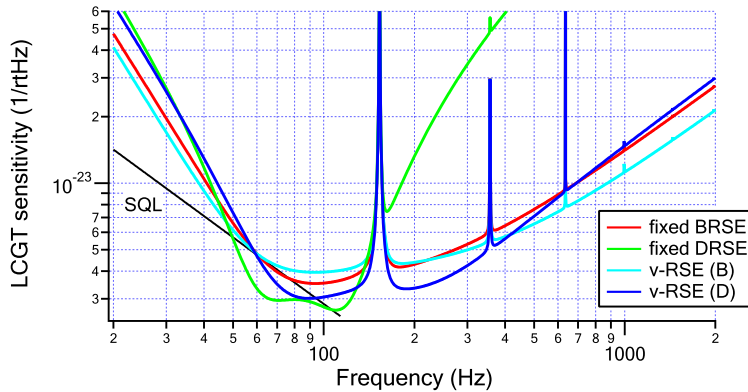


Figure 1: Sensitivity curves of the candidate configurations: BRSE (red curve), DRSE (green curve), and VRSE (B/D) with sky-blue/blue curves.

tational waves as soon as possible, and (2) to obtain astrophysical prospects from the observed waves. For these purposes, a neutron-star binary inspiral event is set to be the primary target of LCGT, because it is a confident source with known waveform and event rate. The observable ranges for this event are 114 Mpc for BRSE, 112/123 Mpc for VRSE (B/D), and 132 Mpc for DRSE (Fig. 2). These ranges are interpreted from scientific outcomes. We set the first minimum success criteria of LCGT as 'to detect at least one event in one-year observation'. For this criteria, the success probabilities are more than 99% for all configurations, which are estimated with expected value of event rate and Poisson distribution. Considering another criteria 'to detect the first event as soon as possible', we estimated the required observation time for the first detection with 90% probability. The results are 5.1 months for BRSE, 5.3/4.0 months for VRSE (B/D), and 3.4 months for DRSE. This result shows that the detuned configurations have advantages in the first detection and expected number of events. On the other hand, broadband configurations are favorable to extract information from observed waveforms, in accuracy of estimated binary parameters, the arrival time, and so on, because wider band provides longer observation duration for an inspiral event. The difference in the accuracy is around a factor of 2 to 4. In addition, broadband configurations have advantages in observation of variety of GW sources, such as signals from supernovae, pulsars, and so on.

Secondary, the candidate configurations are compared from the viewpoint of technical feasibility in constructing and operating the detector. In the optical design, BRSE and VRSE configurations require higher laser power (810 kW) in arm cavities than that of DRSE configuration (360 kW). Since the power in arm cavities is limited by optical loss in mirrors, higher quality mirrors are required in BRSE and VRSE configurations. As for the control of the interferometer, signal extraction and control schemes for BRSE and DRSE have been established with prototype interferometers, as well as investigations with analytical calculations and numerical simulations. VRSE would require additional complexity in signal extraction scheme to be capable both of broadband and detuned configurations. In the interferometer control, DRSE has slightly tight requirement on the noises introduced by controlling interferometer auxiliary degree of freedom; the DRSE configuration has better sensitivity in low frequency band, which can be easily affected by these control noises without careful design of control loops. As described above, each configuration requires some additional technologies and complexities. However, as results of investigations detailed in Section 4, the differences in technical difficulties, the differences in commissioning times, additional complexities are not critical in

Optical parameter sets	BRSE	VRSE (B)	VRSE (D)	DRSE	Comments
	Fixed Broadband	Variable Broadband		Fixed Detuned	
Summary					Scores: 5 (good) – 1 (bad)
Scientific outcomes					
GW detection	4	4	4.5	5	
Scientific information	5	5	4.5	4	
Delectability for various sources	5	5	5	4	
Technical feasibility					
Optics	3.5	3.5	3.5	5	
Control/Calibration	5	4.5	4	3.5	
Commissioning time	5	5	4.5	4.5	
Redundancy	4	5	5	4	
Scientific outcomes					
Neutron–star binary					1.4Msolar neutron–star
Detection probability [%]	99.6	99.4	99.9	99.9	At least one detection with one–year observation
Observation time required for the first event detection [Month]	5.1	5.3	4.0	3.4	With 90% probability
Observable range [Mpc]	114 (259)	112 (255)	123 (281)	132 (299)	SNR 8, sky average SNR 8, maximum direction
Detection rate [/yr]	5.4	5.2	6.9	8.2	One–year observation
Parameter estimation	○	○	○	△	Factor of two difference
Error in arrival time [msec]	0.254	0.220	0.255	1.08	200Mpc events
Fake reduction	○	○	○	△	
Black–hole binary					10Msolar black–hole inspirals
Observable range [Mpc]	570	557	615	677	
Event rate [/yr]		0.07–7			
Black–hole ringdown					
Observable range [Gpc]	2.1	2.0	2.3	3	
Mass range [Msolar]	110–910	115–760	100–490	100–450	Events within 1 Gpc distance
Supernova					
Observation possibility	○	○	○	△	
Event rate [/yr]		0.01 – 0.05			Events in our Galaxy
Pulsar					With one–year observation
Number of observable pulsars	35	38	35	25	Reach spin–down upper limit
Crab upper limits 1e–27	8.5	8.5	8.3	5.9	60Hz
Vela upper limits 1e–27	6.9	6.0	9.3	1.0	22Hz
LMXB 1e–26	1.1	0.95	1.1	14	600Hz
Technical feasibility					
Optical design					
Power in arm cavities [kW]	814	814		362	
Finesse	1550	1550		690	
PRG/SBG	11	11		11	
Tolerance for optical loss [%]	0.54			0.24	Sensitivity Degradation by additional 30ppm mirror loss
PRC, SRC length [m]		73.3			
MC length		13.3			
Interferometer control					
Length sensing	○	○	○	○	
Control noises	○	○	○	△	
Calibration					
Amplitude error	○	○	△	△	
Arrival time error	○	○	○	△	
Commissioning term	○	△	△	○	Small difference
Costs	○	△	△	○	Small difference

Figure 2: Summary of survey results for the candidate configurations.

	BRSE Fixed Broadband	VRSE (B) Variable Broadband	VRSE (D) Variable Detuned	DRSE Fixed Detuned
Scientific outcomes				
Advantage	Wider observation band to cover various GW sources. Better estimation accuracy for parameters of the source.	Flexible observation with both advantages of BRSE and DRSE.		Larger number of event detections are expected with better observable range for neutron-star binaries.
Disadvantage	Worse observation range for neutron-star binary events.	Small degradation in sensitivities in each operation modes.		Some kind of GW sources (supernovae, pulsars) are out of the observation band.
Technical feasibility				
Advantage	Heritages in prototype tests. Simple interferometer control without detuning in cavity lengths.	Redundancy for technical difficulty. Additional options in noise hunting and diagnosis in a commissioning phase.		Heritages in prototype tests.
Disadvantage	Higher quality optics are required.	Additional complexity in signal extraction for the interferometer control. Higher quality optics are required.		Slightly tight requirements for noises caused by interferometer control.

Figure 3: Comparison of the candidate configurations.

these configurations.

Discussions and conclusions

As a result of investigations described above, there is no critical or deciding factor; every configuration would be suitable for the purpose LCGT, and would be technically feasible. With this situation, we recommend the following strategy. We should construct and operate LCGT at first with a VRSE (D) configuration (a variable RSE configuration with a detuned mode), aiming at earlier detection of gravitational-wave signals. There would be no critical difference in technical difficulties and commissioning times. After the first a few or several detections, the variable configuration provides the possibility to change the observation band to broadband, VRSE (B), so as to obtain more information from waveforms, and to observe various targets other than neutron-star inspirals, such as supernovae, pulsars, and so on. In a detector technical point of view, the variable-band configuration is favorable in adding redundancies for unexpected technical difficulties, and in having additional measurement options in noise hunting and diagnostics of the interferometer during commissioning and operation of the detector, at the cost of a little additional complexities in the interferometer control scheme.

In case of technical difficulties in interferometer control system which may be recognized in further investigations, we set BRSE as a backup plan. The BRSE configuration has slightly better sensitivity than VRSE(B), and is considered to have higher technical feasibility.

2 Optical parameter candidates

LCGT has an optical configuration of Resonant-Sideband Extraction (RSE). RSE configuration has been adopted because of its advantages in capability of high laser power in arm cavities and flexibility in observation band. In RSE configuration, we have choices in several optical parameters, such as the observation frequency band, the finesse of the arm cavities, and so on. In this section, we review the baseline design of LCGT with a RSE configuration, and define three candidate optical parameter sets, which are evaluated in the following sections.

2.1 Basic configuration and constraints

The basic concept of LCGT is (1) to have a baseline length of 3 km, (2) with cryogenic test-mass mirrors to suppress thermal noises, and (3) placed at Kamioka underground site for smaller seismic disturbances. The optical configuration of LCGT is designed starting from these boundary conditions.

LCGT has an optical configuration of Resonant-Sideband Extraction (RSE). RSE configuration has adopted because of its advantages in capability of high laser power in arm cavities and flexibility in observation band (Figs. 4, 5 and Table 1). So as to enhance interaction with incident gravitational waves (GWs), and thus, to increase the detector sensitivity to GWs, an interferometric detector should have high laser power in its arm cavities. In a practical detector, the laser power in the arm cavities is limited by optical losses in the interferometer with a given input laser power. An RSE configuration minimizes the optical losses originate in absorption in substrates of optical components (input test masses and the beam splitter), and contrast defect in recombination of beams from two arms on the beamsplitter, by storing most of the laser beam in the arm cavities. Absorption in substrates of input test masses is also a critical issue in LCGT; too much transmission light through the input test mass prevent us to cool it down to cryogenic temperature of 20 K⁴. An RSE configuration enables high power in arm cavities with moderate absorption in ITM.

An RSE configuration has another advantage in flexible observation frequency band. Incident GWs would generate signal sideband components by modulating the laser beam stored in the arm cavities. The signal-extraction cavity (SEC), which is formed by the ITMs and

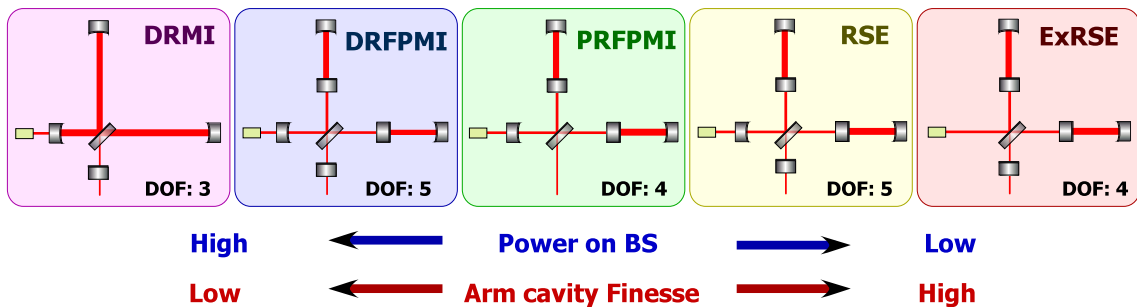


Figure 4: Various interferometer configurations: a dual-recycled Michelson (DRMI) configuration as GEO, a dual-recycled Fabry-Perot-Michelson (DRFPMI) configuration, a power-recycled Fabry-Perot-Michelson (PRFPMI) configuration as LIGO, VIRGO, and TAMA, RSE configuration, and an extreme RSE (ExRSE) configuration which is a RSE configuration without a power recycling mirror.

⁴Capability of the cryocooler for one input test mass is 1 W. Assuming that heat absorption of sapphire substrate is 20 ppm/cm, transmission power through the input test mass (ITM) is required to be less than 1.7 kW (without any safety margin).

Table 1: Comparison between possible optical configurations for LCGT. This table shows technical feasibility scores; score of 5 represents most feasible. LCGT will adopt a RSE configuration as a baseline design.

Config.	BS Pow ¹⁾	ITM Pow ²⁾	Obs. Band	Control	Special requirements
DRMI	1	—	5 (Tunable)	5 (3 DoF)	Cryogenic BS
DRFPMI	2	2	5 (Tunable)	4 (5 DoF)	High power recycling
PRFPMI	3	3	3 (Fixed)	5 (4 DoF)	Powerful cryocooler
RSE	4	4	5 (Tunable)	4 (5 DoF)	
ExRSE	5	5	5 (Tunable)	3 (4 DoF)	High optical gains

¹⁾ Power on the beamsplitter

²⁾ Power transmit through a ITM (Input Test Mass)

the signal-extraction mirror (SEM) at the detection port of the interferometer, extract these signal sidebands from the arm cavities. By adjusting the signal-band gain (determined by the finesse of the SEC) and the detuning phase (determined by the round-trip phase of the signal sidebands in the SEC), the observation frequency bandwidth and center frequency can be tuned for target gravitational waves. Figure 4 and Table 1 shows comparison of feasibility to realize high sensitivity for several optical configurations. From these considerations, we selected RSE as the baseline interferometer configuration of LCGT.

In an RSE configuration, we have choices in several optical parameters: readout phase ζ , ITM power transmittance T (or finesse \mathcal{F}), detune phase ϕ of SEC, and SEM power transmittance T_s . The optimal \mathcal{F} and T_s to maximize the detector sensitivity are quite different between a broadband RSE (BRSE, $\phi = 90$ deg) and a detuned RSE (DRSE, ϕ is optimized for target GW sources) configurations. As it is not easy to replace the mirrors during the observation, we should choose the right setup from the optimized BRSE, optimized DRSE, or one (VRSE) in the middle that performs well in both configurations by changing ϕ . In the following parts, we define the candidates for the interferometer setup of LCGT, referring mainly to its observable distance for neutron star inspirals.

2.2 Broad band configuration

At first, we estimate the detector sensitivity with a broadband RSE configuration. Table 2, 3 shows the mechanical and optical parameters of LCGT that are used to calculate its sensitivity⁵. Thermal noise levels are calculated using those well-known equations from Ref. [1, 2, 3] that are used for other gravitational-wave detectors, except for substrate thermoelastic noise and coating thermo-optic noise, the equations of which are different in the low temperature [4]. The readout scheme is set to be DC readout while RF readout is still an option for the BRSE operation. The readout phase ζ can be tuned by changing amount of the offset in the arm cavity. Here we follow the convention used in Ref. [5]; 90 deg is the phase quadrature for BRSE, where the signal response is maximized. The laser power in the power-recycling cavity (PRC) is set 825 W (75 W input power to the interferometer and with a power-recycling gain of 11).

Figure 6 shows the estimated noise budget of LCGT with a broadband configuration: $\mathcal{F} = 1550$ and $T_s = 0.23$, which gives the highest inspiral range without detuning under the condition that the finesse be 1550 or less⁶. The readout phase is set to be 90 deg. We can see that the sensitivity is not limited by classical noise at most of the frequencies, thanks to low seismic noise in underground and low thermal noise with the cryogenic cooling.

⁵Some of them, for example the beam radius or the suspension wire length, could be modified to reduce thermal noise, but there is a counterpart and the reduction is not so remarkable.

⁶Higher finesse will have difficulty in lock acquisition of the cavity.

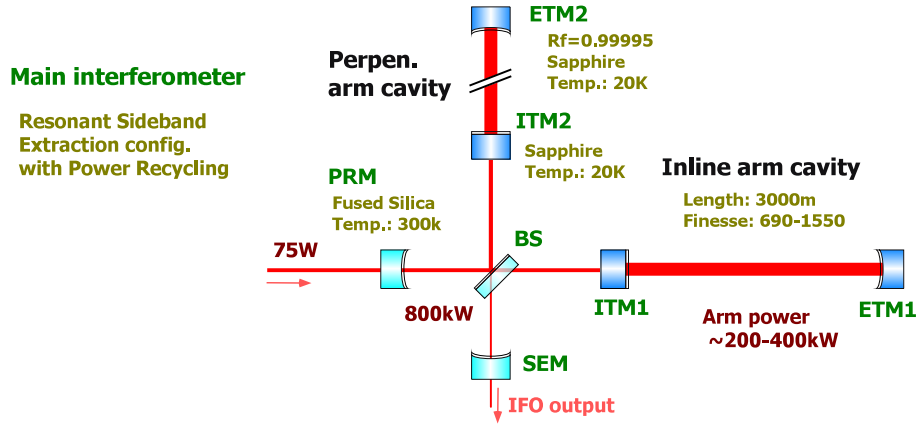


Figure 5: Baseline interferometer configuration of LCGT: a RSE configuration.

Table 2: Main parameters of LCGT

Item	Parameters
Interferometer	
Optical configuration	Resonant-Sideband Extraction (RSE)
Baseline Length	3 km
Input Laser power	75 W (power of carrier beam)
Beam spot size	30 mm
Mirror	
Substrate	Sapphire, Optical absorption 20 ppm/cm
Temperature	20 K
Mechanical loss	1×10^{-8}
Dimensions	Mass 30kg, Radius 125 mm, Thickness 150 mm
Main Suspension	
Material	Sapphire fibers
Number of fibers	4
Temperature	16 K
Mechanical loss	2×10^{-7}
Fiber Dimensions	Length 400 mm, Diameter 1.8 mm

Table 3: Parameters assumed in the sensitivity estimation.

Item	Parameters
Mirror coating	
Silica loss	1×10^{-4}
Tantalum loss	4×10^{-4}
Number of coating layers	9/18
Optical losses	
Optical loss of a mirror	20 ppm
ETM transmittance	30 ppm
Optical loss in SRC	2 %
Quantum efficiency	90 %

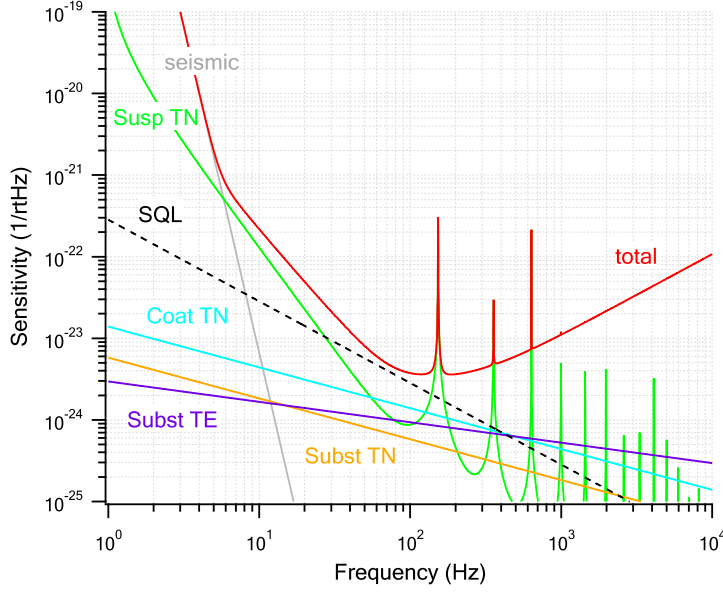


Figure 6: Calculated noise budget of LCGT with the BRSE configuration, the parameters of which is chosen to obtain the highest inspiral range without detuning. The readout phase is set 90 deg.

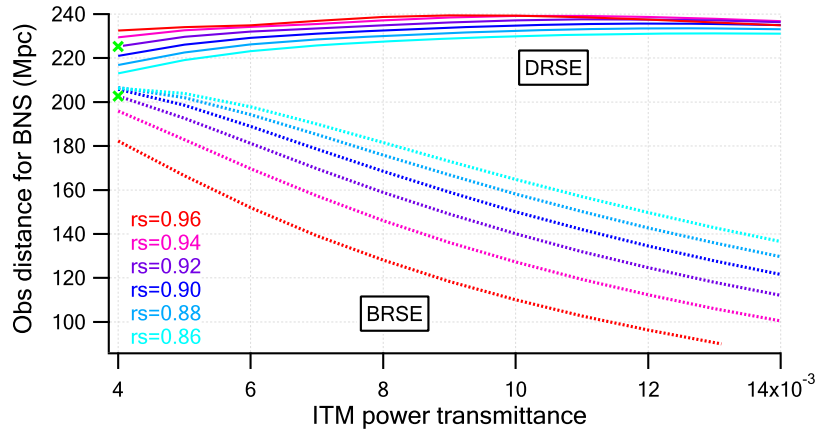


Figure 7: Inspirational range with different finesse (represented by the ITM power transmittance T) and SRM power transmittance T_s . Signal-to-noise ratio is set 8 and the optimal direction (azimuthal incident and best polarization) is assumed. The readout phase for both BRSE and DRSE, and also the detune phase for DRSE is chosen to obtain the highest inspiral range with the given T and T_s . The green crosses indicate the inspiral ranges of BRSE and DRSE with the setup we finally chose.

2.3 Detuned configuration

With detuning, quantum noise can be reduced to raise the inspiral range (IR, the observable range for neutron-star binaries). Figure 7 shows inspiral range of BRSE and DRSE with different \mathcal{F} and T_s . The detune phase of DRSE is chosen to maximize the inspiral range for each \mathcal{F} and T_s . For BRSE, the more the finesse, the higher the range; T_s is to be chosen to optimize the bandwidth for each finesse. For DRSE, decent finesse is rather desirable since there is more room to reduce quantum noise with the optical spring. The highest region of DRSE plots could be damped to be flat without the reduction of thermal noise. The detuning is effective thanks to the cryogenic cooling.

The highest inspiral range is realized with $\mathcal{F} = 690$ and $T_s = 0.08$. The estimated sensitivity curve is shown as the green curve in Fig. 8. The sensitivity curve of this setup is so narrow-band that gravitational-wave signals from other targets like supernovae or LMXB will be hard to observe (detailed in Section 4).

2.4 Variable tuning configuration

As is proposed for Advanced LIGO [6], choosing a setup not to maximize the inspiral range for either BRSE or DRSE alone but to make the best use of both configurations would be a reasonable way for LCGT. In fact, there are many choices in parameter selection. The importance of the inspiral range would not be equal between the BRSE and DRSE configurations.

Taking into account a wide spectrum of factors, we finally picked up a set of parameters for the variable detuning: $\mathcal{F} = 1550$ with $T_s = 0.12$. One can see that the inspiral range for DRSE does not depend much on the selection of T and T_s while it does for BRSE, which is one reason to choose parameters close to the best for BRSE. In addition, the sensitivity at high frequencies with DRSE can be better if the finesse is higher. As is shown in Fig. 8, the VRSE(D) sensitivity is almost as broad as the BRSE sensitivity. The configuration will be chosen between VRSE(D) that is operated with $\phi = 86.5$ deg and $\zeta = 134.7$ deg, and VRSE(B) that is operated with $\zeta = 121.8$ deg to maximize the inspiral range⁷.

2.5 Summary of candidate parameter sets

Table 4 shows brief summary of the setups. In the following sections, we will compare these 3 candidates from various points of view to determine the interferometer configuration of LCGT.

⁷There are the other options to optimize the detune phase and the readout phase for a particular kind of gravitational-wave source. For example, the inspiral range for the 60 solar-mass black-hole binaries can be 30 % higher than with the VRSE (D) configuration if we lower the power to 10 W and use $\phi = 80$ deg and $\zeta = 140$ deg. It will be also an option to optimize the phases for an intermediate operation like a low-power operation or a room-temperature operation. Considering these options, we should better prepare for the phase parameters as tunable as possible, while it brings more control noise that may limit the sensitivity.

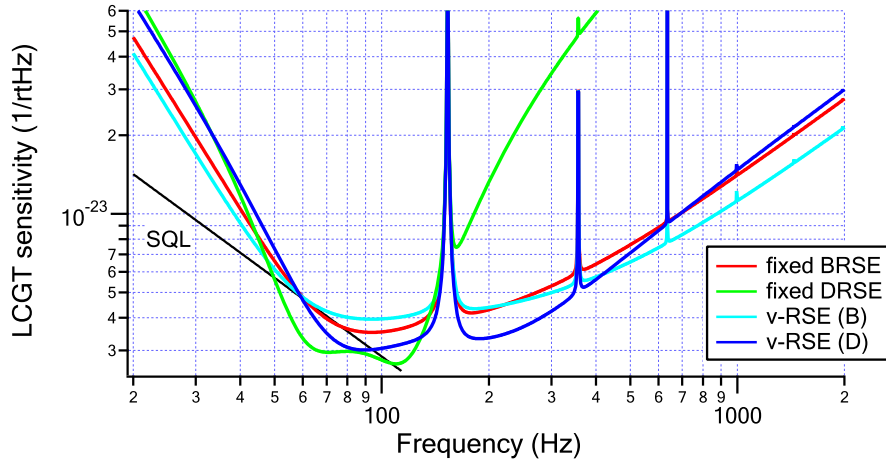


Figure 8: Sensitivity curves of broadband RSE (BRSE), detuned RSE (DRSE), and variable RSE (VRSE). The setup parameters are shown in Table 4.

Table 4: Setup parameters, inspiral range (IR), and strain sensitivity at 1 kHz of each configuration. The first number in each IR column is with the assumption that wave come from the optimal direction for LCGT, and each number in parenthesis is with the average over whole sky.

	T (Finesse)	T_s	ϕ [deg]	ζ [deg]	IR [Mpc]	Sensitivity [Hz ^{-1/2}]
BRSE	0.004 (1550)	0.23	90	127.6	259 (114)	1.4×10^{-23}
DRSE	0.009 (690)	0.08	74.6	103.8	299 (132)	2.1×10^{-22}
VRSE (B)	0.004 (1550)	0.15	90	121.8	255 (112)	1.1×10^{-23}
VRSE (D)	0.004 (1550)	0.15	86.5	134.7	281 (123)	1.5×10^{-23}

3 Scientific outcomes from GW observation

Scientific outcomes obtained from GW observation highly depend on the sensitivity and observation band of a detector. In this Section, we survey possible GW sources which would be targets of LCGT, and show advantages and disadvantages of each candidate interferometer configurations.

The most important criteria in the comparison is to increase the possibility to achieve the minimum success of LCGT: detect at least a few GW events within one year operation. In addition, extracted information from observed waveforms (for example, binary mass parameters) and those accuracies should be considered. The primary target of LCGT is coalescences of neutron-star binaries. Thus, we at first estimate the observable range, expected event rates, required observation period for the first detection, and measurement accuracy of binary mass parameters for these sources. After that, we survey scientific outcomes from the other GW sources: black-hole binaries, black-hole ringdown, supernovae with stellar-core collapses, pulsars. We also compare the candidate configurations from a viewpoint of international observation network.

3.1 Neutron star binary coalescences

Coalescences of neutron star (NS) binary are most promising target sources with known waveforms and reasonable event rates. Here, we estimate the detection probability of these sources.

Expected event rate and detector ranges

The expected detection rate for these events in one year observation is given as

$$\overline{N_{ev}} = \frac{4}{3}\pi d^3/(1+z)^3 \rho_{galaxy} \mathcal{R}, \quad (1)$$

where d is an observable distance of the detector, ρ_{galaxy} is a number density of galaxies, \mathcal{R} is a binary merger rate for milky-way equivalent galaxy, and z is a redshift at range distance. $(1+z)^3$ is a correction for commoving volume. A galactic binary merger rate \mathcal{R} are expected as 82 events per mega-years for milky-way equivalent galaxy [13, 14]:

$$\mathcal{R} = 83.0^{+209.1}_{-66.1} \text{ (C.I. 95\%)} [\text{events Myr}^{-1}].$$

The detection range of the LCGT is determined by the GW event's signal-to-noise (S/N), which is calculated from detector noise spectrum⁸. We define the detection range (the observable distance) d as where GW event's signal-to-noise ratio will be larger than 8 (S/N > 8). The maximum range d_{max} is derived from Eq. (2). According to the antenna pattern of the IFO, a detection range d_{avg} for whole sky average is given as

$$d_{avg} = d_{max} \times 0.44.$$

⁸In the case of the optimal direction (azimuthal incident, best polarization), S/N will be given in following relations (In detail and notations, see [19]):

$$S/N = \sqrt{2} A \left[4 \int \frac{f^{-\frac{7}{3}}}{S_n(f)} df \right]^{\frac{1}{2}} \quad (2)$$

where,

$$A = T_{\odot} \frac{c}{d} \left(\frac{5\mu}{96M_{\odot}} \right)^{\frac{1}{2}} \left(\frac{m}{\pi^2 M_{\odot}} \right)^{\frac{1}{3}} T_{\odot}^{-\frac{1}{6}}, \quad T_{\odot} = \left(\frac{G}{c^3} \right) M_{\odot}, \quad m = m_1 + m_2, \quad \mu = \frac{m_1 m_2}{m},$$

and $S_n(f)$ is average noise spectrum of the detector.

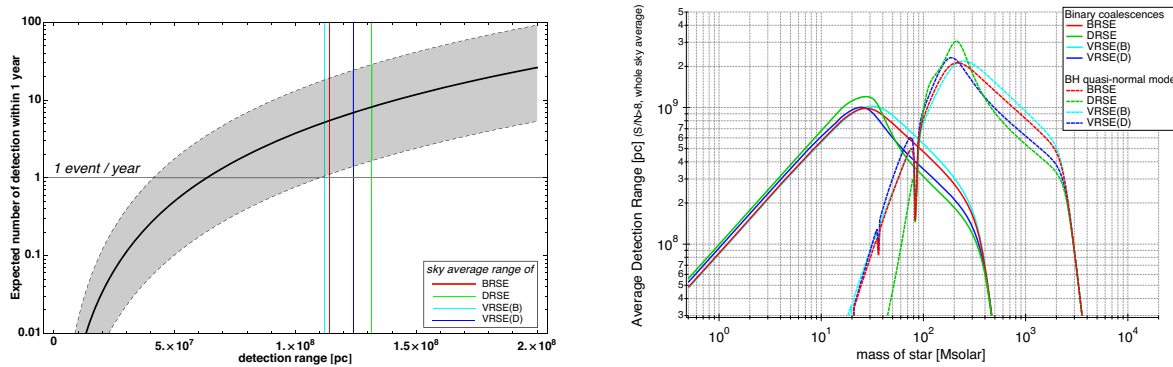


Figure 9: *Left*: Expected event rate \overline{N}_{ev} as a function of sky average detection range. Solid thick black line is \overline{N}_{ev} according to the Eq. (1), and gray shaded zone is a confidence band of 95%. Solid thin lines show the range for binary coalescence. Colors are corresponding to the IFO configurations. *Right*: Sky-averaged detection ranges as a function of mass of the source. Solid lines show the range for binary coalescence. Dashed lines show the range for ringdown GW from black-hole quasi-normal mode. Colors are corresponding to the IFO configurations.

The factor 0.44 convert d_{max} to the radius d_{avg} of a sphere which has same volume of IFO antenna pattern^{9,10}. Figure 9 displays the whole sky average detection range in cases of four proposed IFO configurations. With detuned configuration (DRSE), detection range is better than others for binary mass below $40 M_{\odot}$. We employ the number density of the galaxy as

$$\rho_{\text{galaxy}} = 1 - 1.5 \times 10^{-2} [\text{Mpc}^{-3}],$$

which determined from the B-band luminosity [17, 18]. Figure 9 shows \overline{N}_{ev} as a function of sky average detection range.

Detection probabilities and extracted information

We estimate the probability that LCGT achieve its minimum success of detecting at least one GW signal in one-year observation, assuming Poisson statistics with mean expected events. Figure 10 shows the results: the probability of detection for at least one (and 5, 10) event(s) within one year observation as a function of a detection range. All candidate IFO configurations reach a minimal success requirement; at least one event per year. Left graph of Fig. 11 shows the detection probability as a function of observation period. Table 5 summarize ranges, expected event rates, required observation period for event detection, etc.

Measurement of the source characteristics is an important task in the data analysis. Narrow band configuration (DRSE) is worse as roughly twice of broadband configurations about the accuracy of binary parameters as listed in Table 5. Especially, arrival time accuracy will become important in the determination of the GW source direction.

Estimations in Table 5 suggest that switching between broadband and detuned in variable configuration, VRSE (B/D), has no significant merit and demerit as far as noise spectrum. We must consider with accuracy of the calibration, stableness, commissioning schedule, etc.

3.2 Black-hole binary coalescences

Black-hole (BH) binary coalescences are also interest GW sources. LCGT is able to detect GW's from stellar mass BH binaries (BH-BH or BH-NS). Table 6 summarize the range for these binaries, etc.

⁹The factor also include the effect of GW polarization and inclination of binary orbit plane.

¹⁰The factor 0.44 is determined by the numerical simulation study [21], which assume the threshold of S/N for the detection. The factor is 0.4 with RMS average [20], and $1/\sqrt{5}$ for non-polarized case.

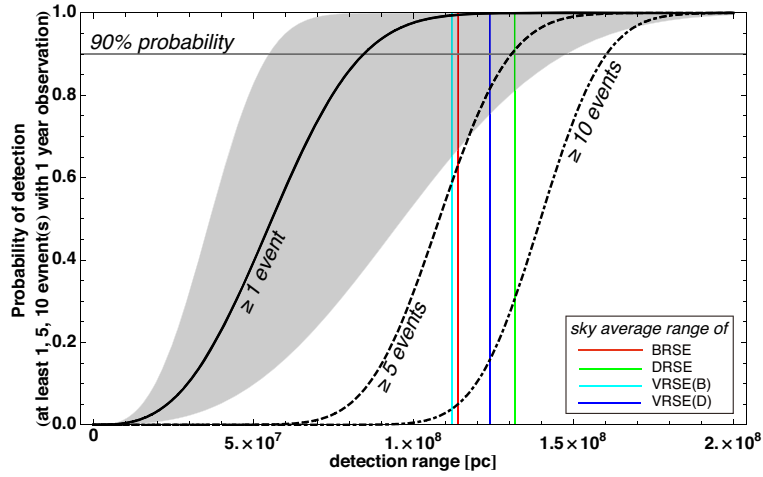


Figure 10: Probability of NS-NS event detection as a function of sky average detection range. Solid thick balck line is a probability of NS-NS event detection, and gray shaded zone is a confidence interval of 95%. Solid thin lines show the range for binary coalescence. Colors are corresponding to the IFO configurations.

Table 5: Summary of comparison of interferometer configurations for NS-NS binary observations

	IFO configurations			
	BRSE	VRSE (B)	VRSE (D)	DRSE
NS Binary ($1.4 - 1.4M_{\odot}$) :				
Detection range d_{avg} [Mpc]	114	112	123	132
(maximum. d_{max} [Mpc])	(259)	(255)	(281)	(299)
Expected observed event rate $\overline{N_{\text{ev}}}$ (C.I. 95%) [events/yr]	$5.4^{+13.7}_{-4.3}$	$5.2^{+13.0}_{-4.1}$	$6.9^{+17.3}_{-5.5}$	$8.2^{+20.6}_{-6.5}$
Probability of event detection				
within 1 year	99.6%	99.4%	99.9%	99.9%
within 6 months	93.4%	92.5%	96.8%	98.3%
within 3 months	74.3%	72.5%	82.1%	87.0%
Observation time for 90% probability of event detection [months]	5.1	5.3	4.0	3.4
Accuracy of source parameters for the event at 200 Mpc away				
S/N	10.4	10.2	11.3	12.0
arrival time δt_c [msec]	0.254	0.220	0.255	1.08
chirp mass $\frac{\delta M}{M}$	2.34×10^{-5}	2.14×10^{-5}	2.77×10^{-5}	3.72×10^{-5}
$\frac{\delta \eta}{\eta}$	0.0045	0.0041	0.0048	0.0098

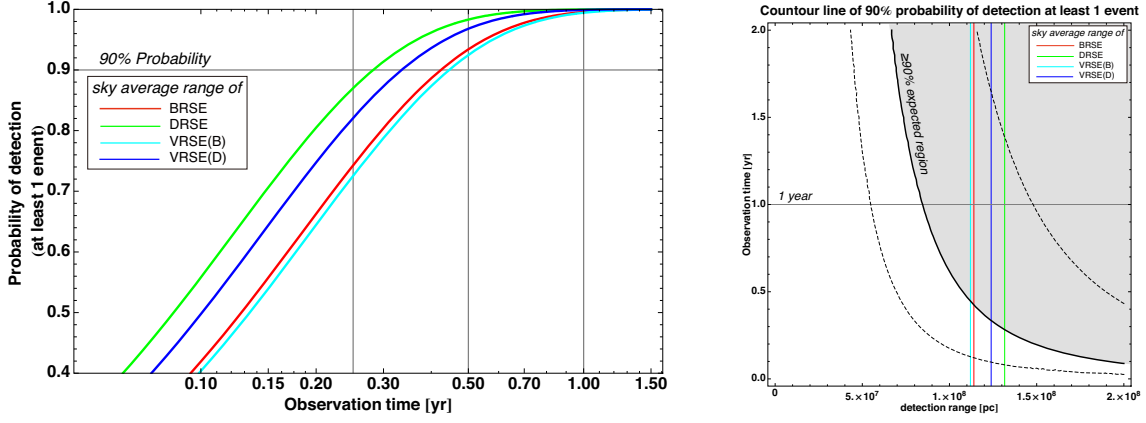


Figure 11: *Left*: Probability of NS-NS event detection as a function of observation periods. Solid thin lines show the range for binary coalescence. Colors are corresponding to the IFO configurations. *Right*: Expected rate \overline{N}_{ev} as a function of sky average detection range. Solid thin lines show the range for binary coalescence. Colors are corresponding to the IFO configurations.

Table 6: BH observations

	IFO configurations			
	BRSE	VRSE (B)	VRSE (D)	DRSE
Binary coalescences NS-BH ($1.4-10M_{\odot}$)				
Detection range d_{avg} [Mpc]	240	235	261	278
Expected event rate [events/yr]		0.006 – 6		
Binary coalescences BH-BH ($10-10M_{\odot}$)				
Detection range d_{avg} [Mpc]	570	557	615	677
Expected event rate [events/yr]		0.07 – 7		
Quasi-normal mode :				
Detection range d_{avg} [Gpc] for $200 M_{\odot}$	2.1	2.0	2.3	3.0
Survey mass region at 1 Gpc [M_{\odot}]	110 - 910	115 - 760	100 - 490	100 - 450

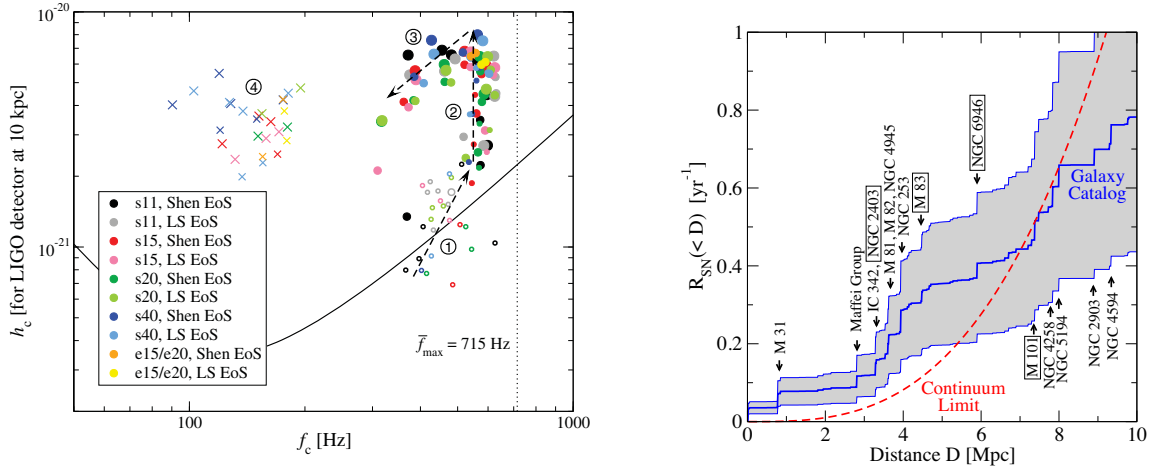


Figure 12: *Left*: GW spectrum of stellar-core collapse. Figure 17 in the reference [24] by Dimmelmeier, et.al. *Right*: Population of supernovae. Figure 1 in the reference [23] by S. Ando et al.

3.3 BH quasi-normal mode

The ringdown GW from quasi-normal mode of black-hole will make it possible to search and to study BH physics. LCGT's detection range and possible survey mass region is listed in Table 6¹¹. All four IFO configuration has long detection range around $200 M_{\odot}$ of BH mass. Broadband configurations, BRSE and VRSE (B), has slightly wider survey region of mass.

3.4 Supernovae with stellar-core collapse

In supernovae explosion, various scenario of GW emission are proposed. Stella-core collapse is a reasonable process to emit the burst gravitational waves with a bounce of the rotating core. As shown in Fig. 12, recent studies estimate its frequency is around 500 - 1000 Hz. For the study of GW from supernovae, we need good sensitivity above a few 100 Hz.

Rate of the supernovae is estimated as Fig. 12. If LCGT has a detection range of 3 – 5 Mpc, an expected rate of the observation will jump to 0.5 event/year.

3.5 Pulsar and LMXB

Figures 13 and 14 shows the strain sensitivity for continuous waves, with integration of long period. Table 7 summarize the sensitivity and possibility of GW detection from the pulsars. LCGT sensitivity will reach at the theoretical maximum arrowed amplitude due to spin down rate for several ten pulsars in known catalogue. Comparing to DRSE, other configurations have 30 ~ 40% better chance for the candidate pulsars. For LMXB, sensitivity around several 100 Hz is necessary.

It is known that a pulsar period may shift suddenly, which is called as a 'glitch'. During 1981-2006, more than 50 pulsar glitches were observed. There are some proposal to explain glitch mechanism. If f-mode oscillation is excited at the glitches, a gravitational wave radiation is expected as

¹¹In this estimation, we assume the amplitude of ringdown GW corresponding to 3% of mass. See reference [22] in detail.

Table 7: Pulsars and LMXB searches

	IFO configurations			
	BRSE	VRSE (B)	VRSE (D)	DRSE
The number of known pulsars which GW amplitude might reach the sensitivity				
1 year	35	38	35	25
10 years	59	63	57	46
Strain h_c sensitivity for typical sources				
Crab (B0531+21, at 60Hz)				
1 year	8.5×10^{-28}	8.5×10^{-28}	8.3×10^{-28}	5.9×10^{-28}
10 years	2.7×10^{-28}	1.9×10^{-28}	2.6×10^{-28}	1.9×10^{-28}
Vela (PSR J0835-4510, at 22Hz)				
1 year	6.9×10^{-27}	6.0×10^{-27}	9.3×10^{-27}	1.0×10^{-26}
10 years	2.2×10^{-27}	2.7×10^{-27}	2.9×10^{-27}	3.3×10^{-27}
LMXBs (at 600Hz)				
1 weeks	1.1×10^{-26}	9.5×10^{-27}	1.1×10^{-26}	1.4×10^{-25}

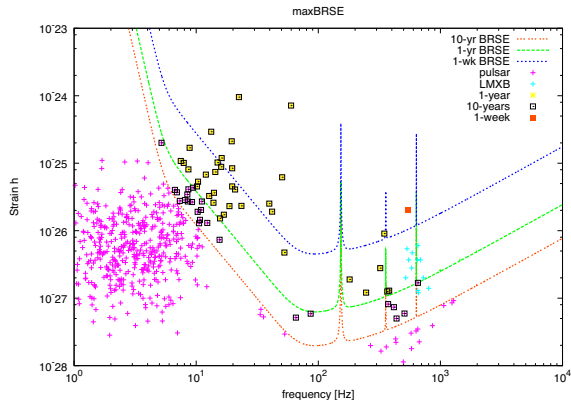


Figure 13: Sensitivity (BRSE) and known pulsars.

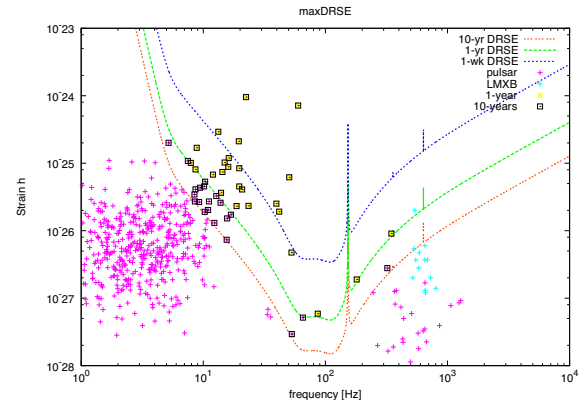


Figure 14: Sensitivity (DRSE) and known pulsars.

$$h = 13.2 \times 10^{-23} \left(\frac{E}{10^{-12} M_{\odot} c^2} \right)^{1/2} \left(\frac{287 \text{ pc}}{R} \right) \left(\frac{2 \text{ kHz}}{f} \right) \left(\frac{0.2 \text{ s}}{\tau} \right). \quad (3)$$

For Vela pulsar, $h = 10^{-22}$, which should be detectable for LCGT except DRSE with high confidence. 16 glitches were observed in 18 years, which means event rate for 0.89 /yr.

$h = 10^{-22}$ for exponential-decay signal at 2 kHz corresponds to $h_{rss} = 1.3 \times 10^{-21}$. BRSE and VRSE(B/D) will be able to search these signal.

3.6 International Network of GW observation

In the most cases of GW searches, we need to employ the world wide network of GW detectors. A simultaneous detection will make possible to determine the source direction, to solve the GW polarization, to exclude spurious events. Hence, we take note affects of IF configuration in the world network analysis.

The accuracy of arrival time in NS-NS binary event is important to decide the source direction. In rough estimation [25], the angular resolution is given as

$$\delta\theta \simeq 4.4 \text{ [degree]} \times \sqrt{\delta t_c \text{ [msec]}} \quad (4)$$

Thus the arrival time accuracy of sub-msec order in one of the detector might dominate the accuracy of the network.

4 Technical Feasibility

In this section, we examine and compare the technical feasibility to realize the target sensitivities with candidate interferometer configurations: fixed BRSE (denoted BRSE), fixed DRSE (denoted DRSE), variable RSE operated in broadband (denoted VRSE(B)) and variable RSE operated detuned (denoted VRSE(D)). For concise comparison of the technical feasibility, the four configurations are compared for above mentioned aspects with scores (Table 8). The scale is from 1 to 10. Larger number means the feasibility is high or the problem is less serious. The scores are normalized column wise, i.e. the best configuration(s) in a column are always given 10.

4.1 Interferometer control

In order to keep an interferometer at its operation point and its best sensitivity, the length between the suspended mirrors must be controlled with precision much better than the laser wavelength. In an RSE interferometer configuration, 5 degrees of length freedom (DoF) should be controlled: L_- , L_+ (differential and common length changes in arm cavities), l_- , l_+ (differential and common changes in the lengths between the beamsplitter and input test masses), and l_s (length of SEC, the signal-extraction cavity). Controlling those degrees of freedom involves two key issues: The first one is the length sensing, which means extraction of length-change information (error signals) from the interferometer using modulation-demodulation schemes. Signals with good separation from other DoF, and with good signal-to-noise ratio (SNR, mainly limited by shot noises) are required. The second issue is control noises. The signals for the central part of the interferometer (l_- , l_+ , and l_s) have worse SNR in general, because of smaller optical enhancement in these DoF with usual interferometer design. Thus, poor design of control loops for these DoF would spoil the interferometer’s sensitivity for GWs in the L_- DoF.

Length sensing

The frontal modulation scheme is widely used in the current interferometric gravitational wave detectors. It has a relatively simple optical configuration requiring only a few modulators in front of the interferometer¹². In order to extract signals for 5 length DoF control, the incident laser beam (the carrier beam) is modulated at two frequencies in its phase (phase modulation, PM) and amplitude (amplitude modulation, AM); the lower-frequency one is called f_1 , and the higher one is called f_2 . These frequencies are selected by resonance conditions of these modulation-introduced sidebands in the interferometer and other constraints¹³; f_1 sideband is

Table 8: Comparison of the technical feasibility. BRSE: fixed BRSE, DRSE: fixed DRSE, VRSE(B): variable RSE operated in broadband, VRSE(D): variable RSE operated detuned. The scores are in the scale from 1 to 10. Larger number is better.

	Control	Mirror loss	Calibration	Commissioning time
BRSE	10	7	10	10
DRSE	6	10	7	9
VRSE(B)	9	7	9	10
VRSE(D)	8.5	7	8	9

¹²There are two candidates for the sensing scheme of the LCGT. One is a variant of the conventional frontal modulation scheme. The other one is called sub-carrier injection method. In this working group, we focused mostly on the frontal modulation scheme. Therefore, the technical feasibility is discussed assuming the use of this sensing scheme in this section. The basic ideas of the sub-carrier injection technique are explained in Section C.

¹³For sufficient response of the photo detectors, the modulation frequency should be roughly less than 50 MHz.

Table 9: Default parameters assumed for the length control investigations. Signal ports are described as AS for the anti-symmetric port, REFL for the reflection port, and PO for a pick-off port. DC and DDM represent homodyne signal detection and double demodulation, respectively.

Item	BRSE	DRSE
Modulation frequency	$f_1 = 11.25$ MHz, $f_2 = 45$ MHz	
Cavity length	PRC 73.3 m, SEC 73.3 m	
Length of MC	13.3 m (or its integer multiples)	
Signal extraction		
L_-	AS DC	
L_+	REFL f_2	
l_-	AS DDM	
l_+	PO f_1	PO f_2
l_s	REFL DDM	PO f_1
Modulation type	f_1 -PM, f_2 -AM	f_1 -PM, f_2 -PM
Control bandwidth*	L_- : 200 Hz, L_+ : 30 kHz	
	l_+ , l_- , and l_s : 50 Hz	
Feed forward gain	l_+ , l_- , and l_s : 30	

*Simple open loop gain of f^{-1} is assumed.

supposed to resonate in the SEC (signal-extraction cavity), and f_1 sideband is supposed to resonate only in PRC (power-recycling cavity). Though, there are wide range of selections in these frequencies and interferometer length parameters, we choose the parameter set¹⁴ shown in Table 9. We assumed a phase modulation - phase modulation (PM-PM) pair for DRSE and phase modulation - amplitude modulation (PM-AM) for BRSE as the first and second modulations. With these modulations and signal ports shown in Table 9, error signals with sufficient separation and SNR can be extracted (details are described in Section B).

Variable detuning

In VRSE configuration, it is required to change the round-trip phase of the laser beam in the SEC. The amount of detuning is adjusted by changing the operation point of l_s , with an additional offset in the l_s control loop. A detuning phase range of 3.4 deg (59 mrad) is required for the candidate VRSE configuration. Since it requires only an addition of an offset electrically, the complexity of the control scheme is the same for all the three configurations (BRSE, DRSE and VRSE). On the other hand, the linearity of the error signal within the tuning range is critical in detuning the phase with an offset to the SEC error signal (l_s). The shape of l_s error signals for the single demodulation (SDM) in the pick-off port, and the double demodulation (DDM) in the reflection port are shown in Fig. 15. In SDM, the detuning phases required for VRSE(B and D) are well within the linear range¹⁵.

Noises from control loops

LCGT has 5 length DoF to be controlled. If a plant has multiple DoF to be controlled, the

In addition, so as to reject the junk lights from modulators, a mode cleaner (MC) should be placed between the modulators and the main interferometer; the modulation sidebands have to pass through the MC. Thus, the choice of modulation frequencies are limited to discrete numbers, depending on the FSR (free-spectrum range) which is inverse proportional to the MC cavity length.

¹⁴Though better parameter sets may be found for each configuration, here we compare the optical configurations with the same control parameters for the simplicity.

¹⁵On the other hand, locking point is out of the linear range for DDM because the detuning phase is too small. This situation might be different if the macroscopic SRC length is adjusted to be resonant for one of the $\pm f_2$.

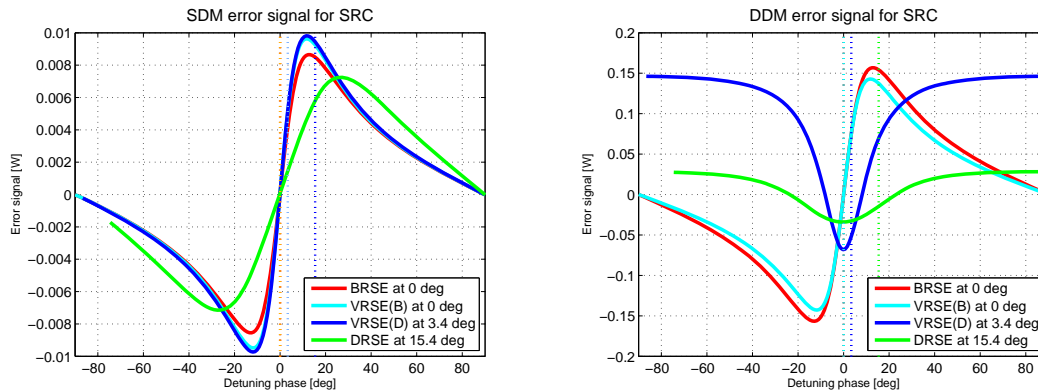


Figure 15: l_s error signals with single demodulation (*Left*) and with double demodulation (*Right*, the signal for DRSE is magnified by 10 times).

shot noises of auxiliary degrees of freedom can contaminate the signal of the main degree of freedom (L_- in our case) through inter-couplings between the sensing signals and the feedback loops. The loop coupling noises depend on the control bandwidth. Here, we assume typical control bandwidth summarized in Table 9¹⁶. In addition, a feed forward (FF) noise cancellation technique onto l_+ , l_- , and dl_s DoF is absolutely necessary to achieve the target sensitivity for gravitational waves. The amount of the canceling is characterized by a parameter called FF gain; we assume the default FF gain to be 30¹⁷.

Figure 16 shows loop coupling noises of 4 configurations. The red curves represent the sensitivity level without loop coupling noises. Loop coupling noises contaminate this original noise level, which is shown as dotted black curves. Only the DRSE noise is contaminated by the loop coupling noise. In this case the culprits are L_+ and l_+ noises¹⁸. Other 3 configurations are free from loop coupling noises above 10 Hz. The effects of loop coupling noises are also evaluated quantitatively in terms of observable range for neutron-star binaries. Reduction ratios of the range by the loop coupling noises are summarized in Table 10.

For the detuned case, the DRSE configuration has the largest susceptibility to the control loop noises. Therefore the actually achievable NS-NS ranges with the loop noise are comparable for the DRSE and VRSE(D) with default FF gain. In other words, DRSE will require higher FF gain to take advantage of its tuned sensitivity (detailed in Section B). This result diminishes the advantage of the fixed DRSE. For the broadband case, the immunity to the loop noise is

Table 10: Observable ranges for neutron-star binaries (optimal direction, SNR=8) with the candidate configurations, and ranges with loop coupling noises.

configuration	BRSE	VRSE(B)	VRSE(D)	DRSE
NS range, original	260.0 Mpc	254.2 Mpc	279.8 Mpc	298.0 Mpc
(Averaged range)	(114.4 Mpc)	(111.8 Mpc)	(123.1 Mpc)	(131.1 Mpc)
NS range for loop noise	258.3Mpc	251.4Mpc	274.8Mpc	266.4Mpc
Ratio of the ranges	99.3%	99.9%	98.2%	89.4%

¹⁶LCGT will be placed in the Kamioka mine which has a very quiet seismic noise environment, so the control bandwidth is not necessary so high.

¹⁷This number is thought not to be so difficult. Advanced LIGO assumes higher FF gain of 100.

¹⁸The main reason why l_+ and L_+ noises are large is that the fineness of arms for DRSE configuration is lower than that of other configurations. DRSE itself is not guilty.

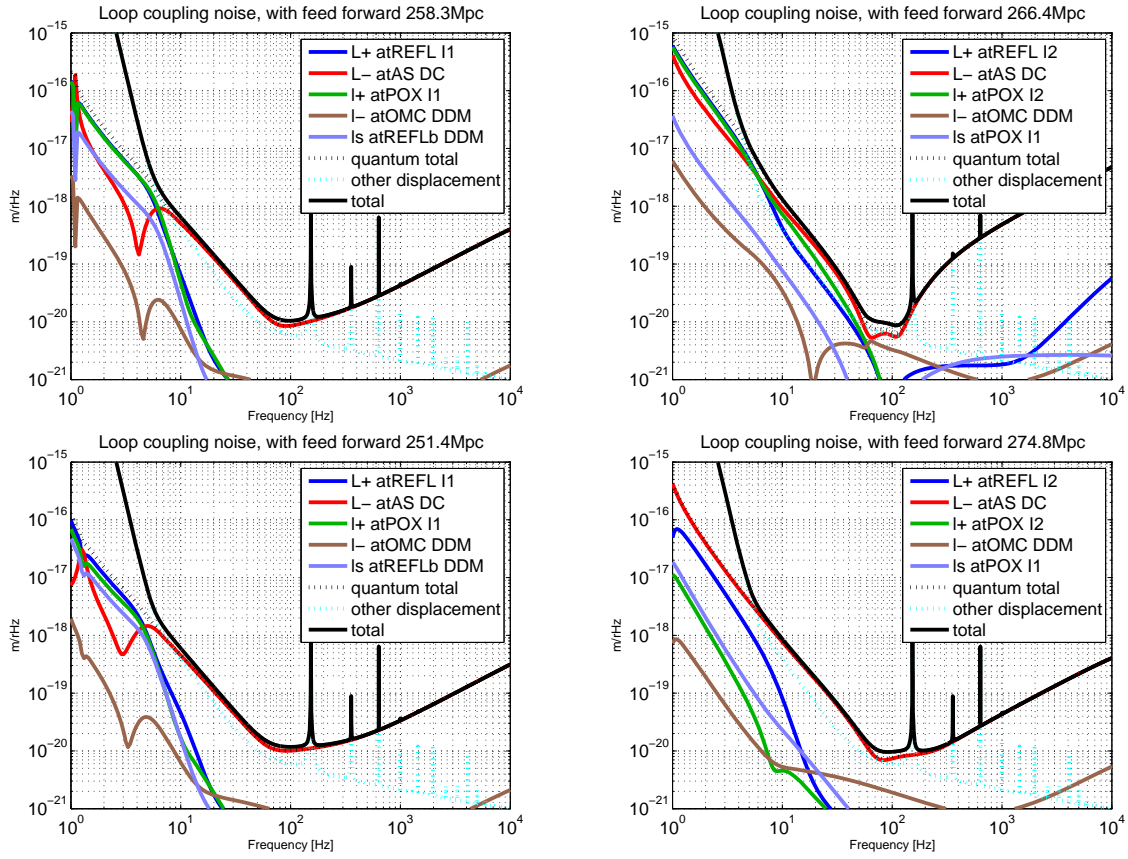


Figure 16: Loop coupling noise of BRSE and DRSE (*Upper left and right*), and VRSE (B and D, *Lower left and right*) .

the same for the BRSE and VRSE(B) cases.

4.2 Mirror loss

The loss of the test mass mirrors affects the sensitivity of an interferometer mainly through the degradation of the power recycling gain. Higher finesse cavities are more susceptible to additional losses. Among the four candidate configurations, only the DRSE has a different finesse. Since it has a much lower finesse than the others, the DRSE is less affected by unexpected loss increase in the mirrors.

The optical gain of a Fabry-Perot cavity is roughly described as $1/\mathcal{L}$, where \mathcal{L} is a round-trip optical loss in the cavity. Here we consider that the arm cavity is formed by ETM (end test mass), and a compound mirror with ITM (input test mass) and PRM (power-recycling mirror). In BRSE and VRSE configurations, the total power inside the arm cavities will be 814 kW, which is larger than the incident laser power by 1.1×10^4 times. This ratio corresponds to a requirement for a round-trip optical loss \mathcal{L} of 92 ppm in reflection at ETM and a compound mirror with by ITM and PRM. In the DRSE case, the power ratio is 4.8×10^3 , which corresponds to a loss requirement of 200 ppm.

4.3 Calibration

The optical gain of DRSE interferometer shows a complex frequency response compared to BRSE. The shape of the response depends on the easy-to-change parameters such as detuning phase, homodyne phase, laser power etc. Therefore, we have to monitor the loop gain at several frequencies during the observation to keep track of the optical gain changes. Especially in the case of VRSE(D), the detuning phase can vary with the laser power fluctuation. Therefore, the calibration has to be done more carefully.

In contrast, the optical gain of the BRSE is characterized only by the overall gain and the cavity pole frequency. Since the cavity pole should not change much during the operation, we only have to monitor the overall gain. This is much simpler than DRSE.

5 Project strategy

5.1 Commissioning time

The estimation of commissioning time is a critical issue in the selection of interferometer configuration. Even if the sensitivity for GW signals is better, it is not favorable if it takes a lot of commissioning time. As described in Section 3, differences in the required observation time for the first GW detection is 2 months at most. Thus, we evaluate the deference in commissioning time in this time scale. The followings are the current best guesses for the commissioning time.

The behavior of the interferometer is simpler for broadband operation, because the sidebands are all balanced and there is no optical spring nor RSE peaks. Moreover, the peak sensitivity is slightly better for detuned configurations than the broadband ones. This means that we may need an extra commissioning time to reduce noises other than the optical readout noises below this peak sensitivity level. As for the VRSE configuration, the addition of offset to the SEC signal to detune the cavity could introduce some technical problems since the f_1 sideband is not fully resonant in the SEC. If we choose the SEC length to be optimized for VRSE(B) (i.e. f_1 is resonant in the SEC for broadband operation), the VRSE(D) configuration may suffer from this problem. If we optimize the SEC length for VRSE(D), VRSE(B) will suffer in turn. We do not see any fundamental difference between BRSE and VRSE(B) if the SEC length is optimized for VRSE(B). Although the detuned configurations may require some extra commissioning time, which we consider it to be small with a careful construction scheduling.

In summary, though the commissioning time will be different in candidate configurations, the difference is not so significant (Table 8).

5.2 Cost comparison

The difference in cost is another factor to determine the optical configuration. The differences could originate in mirror quality and additional instruments for interferometer control (modulators and electronic devices). However, in the current estimation, the differences in cost for candidate configurations will be negligible compared with the total cost of LCGT.

5.3 Risks in noise hunting and diagnosis

Difficulties in the noise hunting during the commissioning phase, and diagnosis during the observation would be an additional risk to keep the commissioning schedule and to realize the designed sensitivity. The response of broadband interferometers would be simpler than the detuned configuration, without additional offset in the resonance or anti-resonance condition of cavities. Moreover, the variable-band configuration has additional measurement options in noise hunting and diagnostics of the interferometer.

5.4 Potential for future upgrades

After the achievement of the original purposes to detect GW signals and to obtain scientific results, LCGT would have a chance to upgrade the detector¹⁹. This upgrading may contain replacements of components (mirrors and laser source), installation of new subsystems (equipments to reduce quantum noises). None of the candidate configurations excludes the possibilities of theses upgrades.

¹⁹We assume that this upgrade is in several years after the start of observation.

A Special Working Group members

Cordinator: Seiji Kawamura (NAOJ)

Chair: Masaki Ando (Kyoto University)

Members:

Nobuyuki Kanda (Osaka City University)
Yoichi Aso (University of Tokyo)
Kentarō Somiya (Caltech)
Osamu Miyakawa (ICRR)
Hideyuki Tagoshi (Osaka University)
Daisuke Tatsumi (NAOJ)
Hiroataka Takahashi (Nagaoka University of Technology)
Kazuhiro Hayama (AEI)
Kazuhiro Agatsuma (NAOJ)
Koji Arai (Caltech)
Kiwamu Izumi (NAOJ)
Yuji Miyamoto (Osaka City University)
Shinji Miyoki (ICRR)
Shigenori Moriwaki (University of Tokyo)
Shigeo Nagano (NICT)
Noriaki Ohmae (University of Tokyo)
Shuichi Sato (Hosei University)
Toshikazu Suzuki (KEK)
Ryutaro Takahashi (NAOJ)
Takashi Uchiyama (ICRR)
Hiroaki Yamamoto (Caltech)
Kazuhiro Yamamoto (AEI)

and the LCGT Observation Band Special Working Group.

B Interferometer Sensing and Control Scheme

The original LCGT sensing and control scheme was designed for BRSE configuration. Therefore, we have to find a new scheme to control a variable detuning RSE interferometer. In this section, we will examine a variant of the conventional frontal modulation scheme, where we apply phase or amplitude modulations to the carrier light at two frequencies. The lower one is called f1 and is supposed to resonate in the SRC. The higher one is called f2 and is resonant only in the PRC.

B.1 Sideband resonant conditions

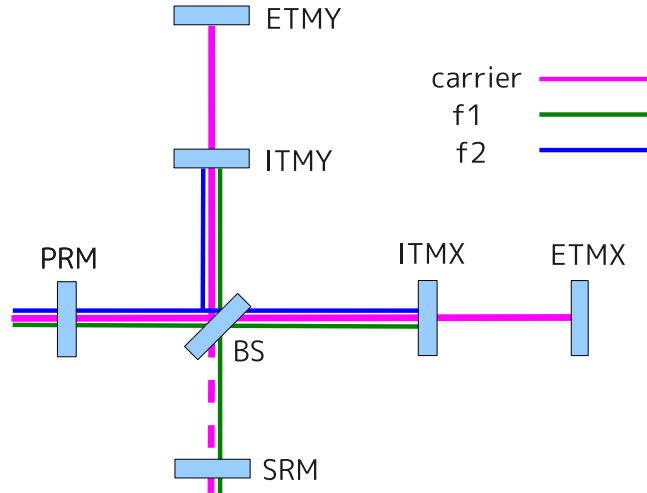


Figure 17: Resonant conditions for the carrier and sidebands

Figure 17 shows the resonant conditions for the carrier and the sidebands. The carrier has to resonate in the PRC and the arm cavities. The anti-symmetric port of the Michelson is kept dark for the carrier and f2 so that they are all reflected back to the symmetric port. The Schnupp asymmetry and the f2 frequency are chosen so that the MICH reflectivity for f2 is 1. With this configuration, f2 only sees the PRC and is not affected by the motion of the SRM. The f1 sideband has a finite transmissivity through the Michelson part and resonates in the SRC. It is this sideband which carries the information of the SRC length change.

Since the SRC is controlled to resonate the f1 sideband inside, the amount of detuning for the carrier (i.e. the resonant condition of the carrier in the SRC) is determined by the macroscopic length of the SRC. We can also change the SRC detuning by adding an offset to the error signal for the SRC length control.

In order to change the detuning phase, we apply an offset to the SRC error signal to move the SRC length microscopically. For this purpose, the resonance of the SRC to f1 should have an appropriate bandwidth to allow us to extract a linear signal over the desired detuning range. If the resonance is too sharp, we won't have an enough range for detuning by an offset. If the resonance is too wide, the SRC signal may decrease as we don't get a large enhancement of the phase change inside SRC by multiple bounces.

The sharpness of the SRC resonance (finesse) is determined by three parameters, PRM reflectivity (r_p), SRM reflectivity (r_s) and the Michelson reflectivity to f1 (r_{m1}). Of the three parameters, two (r_p and r_s) are pre-determined to optimize the bottom line sensitivity of the LCGT. Therefore, we are left with r_{m1} to change the finesse.

For r_{m1} to be an effective mean to change the SRC finesse, f1 has to be resonant to PRC. When this condition is satisfied, the effective reflectivity (r_{prm}) of the cavity formed by PRM and the Michelson part is determined by r_{m1} . If r_{m1} is close to r_p , r_{prm} will go down. The higher r_{prm} is, the higher the finesse of SRC. The value of r_{m1} can be chosen by changing the Michelson asymmetry for f1.

With these considerations in mind, we chose the macroscopic length parameters of LCGT with the following steps:

1. Choose the frequency of f2. It should not be too high because then we cannot use large PDs for signal detection. This limit is especially stringent on QPDs used for WFS. If it is too low, the frequency of f1 will also be very low. We do not want to use modulation frequencies below 10 MHz because there, the intensity noise may not reach the shot noise limit. We chose 45 MHz as the default f2 frequency.
2. The PRC length (L_p) and the Schnupp asymmetry L_{as} are chosen to resonate the f2 sideband inside the PRC. The Michelson reflectivity for f2 (r_{m2}) has to be either 1 or -1. Depending on the sign of r_{m2} , the f2 frequency has to be either an integral or half-integral multiple of the FSR of PRC. We also have to take into account the extra sign flip of carrier from the arm cavities to which it is resonant, when considering the resonant condition of the sidebands in the PRC.
3. There are many possible combinations of L_p and L_{as} which satisfy the above condition. However, there are several constraints to the lengths. The PRC length is desired to be around 80 m. Since we have 20 m long cryo-shield parts in the vacuum tubes between the BS and ITMs, the PRC length has to be longer than this. In addition to this 20 m, we have to accommodate the Schnupp asymmetry. Although it is not yet decided, it is likely that we have a folded PRC. 50 m or so should be reserved for the folding. From the point of view of the construction cost, we don't want to make the PRC too long. The Schnupp asymmetry should not be too long because we do not want to introduce an excessive mismatch between the two recombining beams.
4. We choose the f1 frequency to make it resonant in the PRC. For a given set of L_p and L_{as} , there are several f1 frequencies which satisfy this condition. First of all, we make f1 lower than f2. Then we pick frequencies with Michelson reflectivity, r_{m1} , close to the desired value. Finally, both f1 and f2 frequencies have to be integral multiples of the FSR of MC. Therefore, the ratio of f1 and f2 determines the MC length. Since we do not want to make the MC too long for the construction cost and the back scattering problem, we choose a frequency which gives a short MC length. Practically, the MC length less than 30 m would be reasonable.
5. The SRC length (L_s) is chosen to make f1 resonant in the SRC at a desired detuning phase of the carrier. We can elongate L_s by $c/(2f1)$ keeping the same resonant condition. We chose L_s to be around 80 m.
6. We scanned the length parameters to find a set of parameters which satisfy all of the above constraints.

Length parameters The table 11 show the candidate parameter sets for LCGT. The set from 1 to 4 are shown in the order of SRC detuning range from narrow to wide. Set 5 is different from the other four in a sense that f1 is not resonant in the PRC in the absence of the SRM for this parameter set. In this case, the reflectivity of the power-recycled Michelson part seen from SRM is that of an anti-resonant cavity. Therefore the detuning range is the smallest with the parameter set 5.

Name	f1	f2	L_p	L_{as}	L_s	L_{MC}
Set 1	12.8571 MHz	45MHz	81.6102 m	6.66205 m	69.9516 m	23.3172 m
Set 2	9 MHz	45MHz	74.9481 m	6.66205 m	74.9481 m	16.6551 m
Set 3	13.5 MHz	45MHz	83.2757 m	3.33103 m	61.0688 m	33.3103 m
Set 4	11.25 MHz	45MHz	73.2826 m	3.33103 m	73.2826 m	13.3241 m
Set 5	14.8 MHz	37 MHz	81.025 m	4.05125 m	81.025 m	20.2562 m

Table 11: Length parameter candidates.

Figure 18 to figure 22 show the power of f1 sideband in the SRC and at the reflection port along with the phase at the pick-off port and the reflection port as the SRC detuning phase is changed. The power is represented as the ratio to incident power. We can see that the resonance width is changed as r_{m1} is changed.

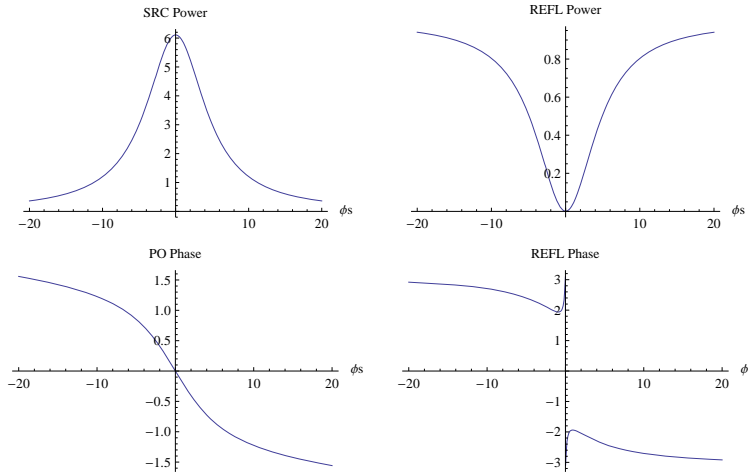


Figure 18: SRC resonance curves for Set 1

B.2 Optickle simulation

Based on the length parameters found above, here we try to find a suitable set of signal extraction ports and demodulation quadratures including double demodulation. Our criteria for this search is that the shot noise and the degeneracy of the signals have to be small enough that the noises coupled to the gravitational wave channel through the control loops do not contaminate the target sensitivities.

Calculations in this section are based on simulated models using the Optickle, frequency domain interferometer simulator which can investigate quantum effect such as radiation pressures and vacuum injections. Here we assume to use Set 4 shown in Table 11, $f_1 = 11.25$ MHz $f_2 = 45$ MHz since this set provides widest linear range for detuning. Better parameter sets for each optical configuration may be found, but here we compare the optical configurations with the same control parameters for the simplicity. We leave the discussion for detailed control method to the interferometer sensing and control investigation team. Newly added parameters or already included parameters in previous section but important for the length control are listed in Table 12. Other parameters are the same as previous sections.

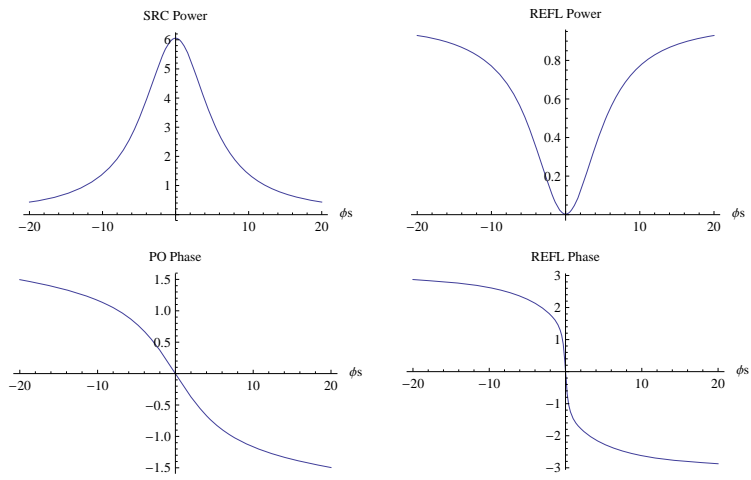


Figure 19: SRC resonance curves for Set 2

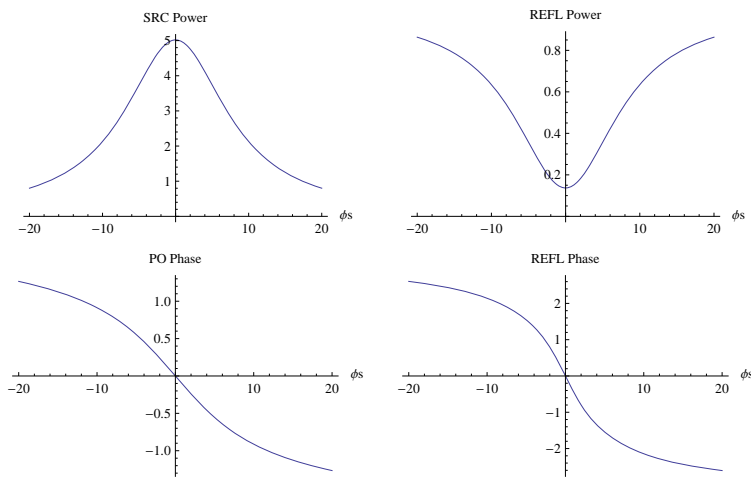


Figure 20: SRC resonance curves for Set 3

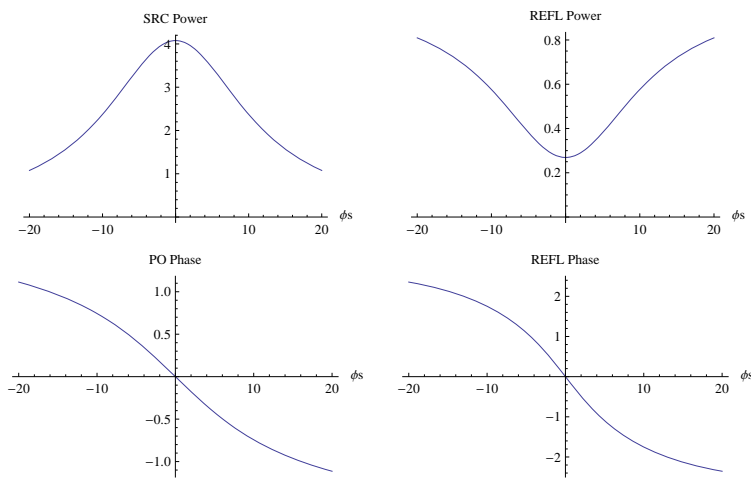


Figure 21: SRC resonance curves for Set 4

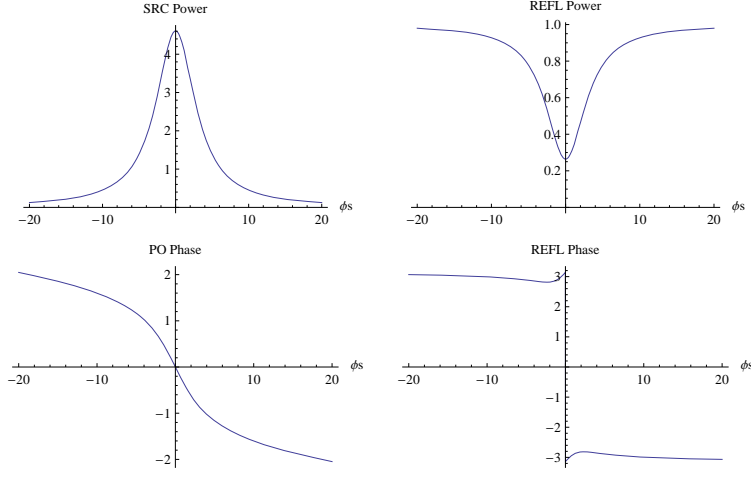


Figure 22: SRC resonance curves for Set 5

Item	Parameters
Modulation frequency	$f_1 = 11.25 \text{ MHz}$ $f_2 = 45 \text{ MHz}$
Modulation depth for BRSE	0.15(PM)-0.1(AM)
Modulation depth for DRSE	0.15(PM)-0.15(PM)
Loss asymmetry	$\pm 15 \text{ ppm}$ at ETM
Arm asymmetry	$\pm 1\%$ at ITM transmissivity
Maximum input power for photo detector	100mW
Control bandwidth	30k, 200, 50, 50, 50Hz for L_+ , L_- , l_+ , l_- , l_s
Feed forward gain	30, 30, 30 for l_+ , l_- , l_s

Table 12: Default parameters assumed for the length control in this section.

B.2.1 Detuning range for signal recycling cavity

When we develop a variable bandwidth RSE, the first question will be how difficult or how easy to obtain a linear signal for l_s to exchange configurations from BRSE to DRSE. There are two ways to establish a variable RSE. One way is just to acquire lock BRSE or DRSE initially. Another way, which is probably more difficult, to exchange bandwidth smoothly from BRSE to DRSE or DRSE to BRSE. In any case, wider linear l_s ranges are better for control but the wider ranges generally mean worse optical gains.

We assumed phase modulation - phase modulation (PM-PM) for DRSE and phase modulation - amplitude modulation (PM-AM) for BRSE as the first and second modulation. Firstly we hope to avoid AM because AM loses carrier power at a modulator much more than that of PM. On the other hand, we need to use DDM not only for l_s but also for l_+ or l_- to avoid degenerations from arm cavity signals (explained later). For DRSE, the detuning makes unbalanced sidebands so that DDM can produce meaningful signals even using PM-PM. However for BRSE, we must use AM to extract useful DDM signals because only beat between AM and PM can produce the useful DDM signals since the unbalanced sidebands do not exist in the BRSE configuration. The shape of l_s error signals for the single demodulation (SDM) and the double demodulation (DDM) are shown in Fig. 15. Note that the DDM signal for DRSE is magnified by 10 times, so this slope is much smaller than other signals. And also DRSE has another difficulty that the locking point is at the edge of the signal for SDM. These difficulties come from that the detuning phase is large and the f_2 won't be resonant anymore in SRC. In other words, the large detuning phase burdens the locking and the signal extraction for l_s . A small detuning like vRSE(D) is fine for SDM but the locking point is out of the linear range for DDM because the detuning phase is too small, an opposite reason from the DRSE. This situation might be different if the macroscopic SRC length is adjusted to be resonant for one of the $\pm f_2$, but we do not discuss the detail for macroscopic length change here. For BRSE, the slope of DDM is more than 10 times larger than that of DDM. Results are summarized in Table 13. From these results, we assume default signals as SDM for BRSE and DDM for DRSE in the following discussion. Using these signals makes it possible to lock both BRSE and DRSE configurations and exchange each configurations smoothly by adding an offset on their error signals.

Configuration	BRSE	VRSE(B)	VRSE(D)	DRSE
locking phase	0deg	0deg	3.4deg	15.4deg
l_s by SDM	$0 \pm 5\text{deg}$ $0 \pm 6\text{mW}$	$0 \pm 5\text{deg}$ $0 \pm 7\text{mW}$	$0 \pm 5\text{deg}$ $0 \pm 7\text{mW}$	$0 \pm 18\text{deg}$ $0 \pm 6\text{mW}$
l_s by DDM	$0 \pm 6\text{deg}$ $0 \pm 120\text{mW}$	$0 \pm 6\text{deg}$ $0 \pm 110\text{mW}$	$10 \pm 6\text{deg (bad)}$ $55 \pm 15\text{mW}$	$19 \pm 10\text{deg}$ $-5 \pm 2.5\text{mW}$

Table 13: Linear phase range (upper line in each column) and linear slope range (lower line in each column) for l_s error signal. The linear range is shown as the center of linear range \pm one side linear range.

B.2.2 Selection of signal extraction ports

It is important to select proper signal extraction ports for the length control. An interferometer provides a lot of ports, but the number of proper ports is not so many. For example, if we use a DC readout method the DC signal of anti symmetric (AS) port is the only one choice for L_- , and a reflection port of the output mode cleaner (OMC)²⁰ is also the only one choice for l_- .

²⁰It is known that the second or third candidate at pick off port with Q-phase or reflection port with Q-phase single demodulation produces very small signal and the shot noise limited sensitivity is much worse.

configuration	L_+	L_-	l_+	l_-	l_s
BRSE	REFL f_2	DC	POX f_1	OMC DDM	REFL DDM
DRSE	REFL f_2	DC	POX f_2	OMC DDM	POX f_1

Table 14: Selected ports for length signal sensing. Names of ports; REFL:reflection port, DC:DC readout at anti symmetric port, POX:pick off port of X-arm, OMC:OMC reflection port. f_1 and f_2 are demodulations with the first and second modulation frequencies.

Ports which have a low shot noise limited sensitivity should be selected firstly. However if the ratio of two signals are similar at two ports these two signals are degenerate and it will be difficult to obtain a good signal separation. It sometimes happens when both two signals are extracted from SDM, for example, L_+ and l_+ or L_+ and l_s . In such a case, this degeneracy appears as a huge loop noise later. We need to select DDM signals even the shot noise limited sensitivity is not so good when signals are degenerate. Here, we assume to use a DC readout method for L_- signal extraction because of a disadvantage of non-stationary shot noise with RF readout and an advantage of possibility of quantum non demolition measurement with DC readout. Table 14 shows a list of selected ports. These ports are almost optimized for each optical configuration, but not perfectly optimized since the parameter space is huge.

B.2.3 Loop coupling noise

LCGT will have 5 length degrees of freedom (DOFs) for an RSE configuration. If a plant has multiple DOFs with their control, couplings of sensing signals exist and their shot noises are fed back as newly induced actuation forces through the feedback loops. In other words, if there are branches at the signal sensing (For example, l_- signal exists in L_- port with a ratio of 1/finesse in principle.) an effective optical gain will be reduced through this branch of the loop. Finally, these loop couplings appear as noises at gravitational wave detection port.

The loop coupling noises depend on the control bandwidth. LCGT will be placed in the Kamioka mine which has a very quiet seismic noise environment, so the control bandwidth is not necessary so high. Here, we assume typical control bandwidth as the unity gain frequency as 30kHz, 200Hz, 50Hz, 50Hz, 50Hz for L_+ , L_- , l_+ , l_- , l_s respectively and simple open-loop gain of just f^{-1} .

We learned from the first generation gravitational wave detector like TAMA or LIGO that a kind of feed forward noise cancellation technique is absolutely needed to realize an acceptable sensitivity for gravitational waves. We call it feed forward (FF) technique in this report and it reduces non-diagonal component in optical gain matrix. We introduce this FF technique onto l_+, l_-, l_s DOFs and this effect is shown as one parameter called FF gain. We assume typical FF gain as 30 which reduces non-diagonal components of optical gain matrix for l_+, l_-, l_s to L_- by factor of 30 in all frequency. Realization of this number is though as not so difficult since Advanced LIGO assumes higher FF gain as 100.

Figure 16 show loop coupling noise of 4 configurations. If no loop coupling noise is not taken into account the total quantum noise will be the same as the original L_- noise calculated from the vacuum noise divided by the optical gain at DC readout port. Other loop coupling noises contaminate this original L_- noise and increase effective L_- noise curve shown as dotted black line. Here only DRSE total noise is limited by the loop coupling noise for L_+ and l_+ noise. Other 3 configurations are free from loop coupling noises above 10Hz.

B.2.4 Reduction of NS-NS binary range by loop coupling noise

Here we summarize NS-NS binary ranges and reduction ratios of the NS-NS binary range by the loop coupling noises for 4 optical configurations in Table 15. A reduction ratio is defined as NS-NS binary range with loop noise divided by NS-NS binary range with no RF modulation. In this calculation, the demodulation phases, detuning phases and homodyne phases (as the offset on end mirrors) are optimized. Demodulation phases are chosen to maximize a desired signal at each port. From these results, it appears that larger detuning phase has larger loop coupling noise.

configuration	BRSE	VRSE(B)	VRSE(D)	DRSE
NS range, no RF(max)	260.0Mpc	254.2Mpc	279.8Mpc	298.0Mpc
NS range, no RF(avg)	114.4Mpc	111.8Mpc	123.1Mpc	131.1Mpc
NS range for loop noise, no FF(max)	142.1Mpc	129.2Mpc	61.0Mpc	33.4Mpc
loop noise, no FF/no RF	54.7%	50.8%	21.8%	11.2%
NS range for loop noise with FF(max)	258.3Mpc	251.4Mpc	274.8Mpc	266.4Mpc
loop noise with FF/no RF	99.3%	99.9%	98.2%	89.4%

Table 15: NS-NS binary range and the reduction ratio.

It is useful to check how safe or robust these configurations if we change the parameters which determine the control loop coupling noises. We will see NS-NS ranges and the reduction with swept parameters then. Figure 23 and 24 show dependence of the NS-NS binary range and the reduction ratio for each optical configuration on the unity gain frequency as the control bandwidth. These results tell us that closer to BRSE is more robust for the increase of control band width. Figure 25 and 26 show dependence of the NS-NS binary range and the reduction ratio on the feed forward gain. These results show also that closer to BRSE is more robust for the reduction of FF gain.

At the last, we see an optimization for the homodyne phases on the simulation models. In the previous section, homodyne phase was optimized analytically. Here setting of the homodyne phase is realized by changing a microscopic offset on two end mirrors differentially. It should be investigated that the possible offset can be applied actually since too large offset may introduce bad asymmetries on the interferometer and it causes a reduction of optical gain or an increase of loop coupling noise. Fig 27 and 28 show relationships between an ETM offset and a NS-NS range. All NS-NS range is optimized around 10^{-12} m which is thought that it is not so difficult to be realized.

C Sub-carrier injection scheme

A rather different scheme for the extraction of the SRC length information with a variable detuning capability was proposed in the working group. The scheme is called “sub-carrier injection” because it makes use of the injection of a secondary laser with the orthogonal polarization to the main laser. Since the study on this scheme is still in its early stage, we only present the basic ideas of the scheme briefly in this section.

The conceptual design of this scheme is shown in figure 29. We use an auxiliary laser with the orthogonal polarization to the main laser to sense the SRC length. This laser is phase locked to the main laser with a frequency offset. Then the sub-carrier is phase modulated to add sidebands and combined with the main laser beam through a PBS before the second MC. We add two sidebands to the sub-carrier. One is not resonant to the MC and used to lock the sub-carrier to the MC. The other one goes through the MC but not resonant in the main

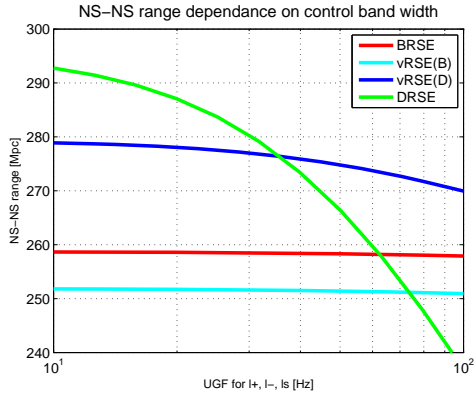


Figure 23: Dependence of the NS-NS binary range on the unity gain frequency.

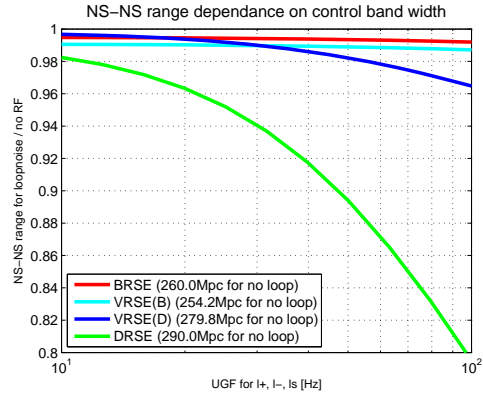


Figure 24: Dependence of the reduction of the NS-NS binary range on the unity gain frequency.

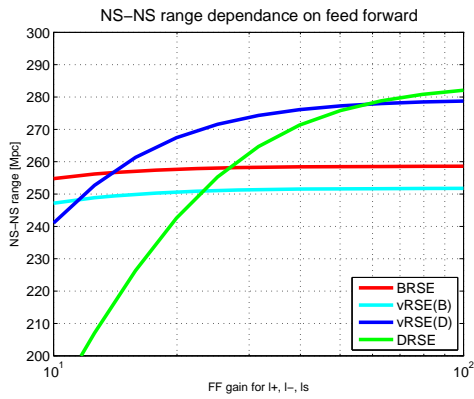


Figure 25: Dependence of the NS-NS binary range on the feed forward gain.

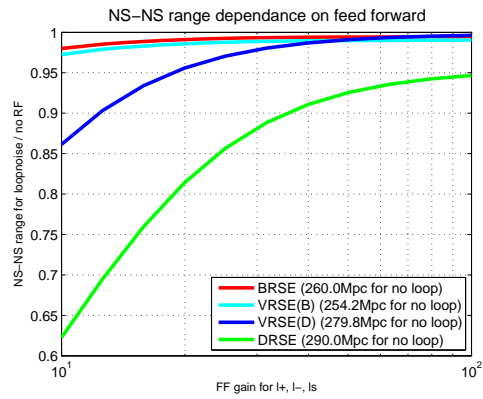


Figure 26: Dependence of the reduction of the NS-NS binary range on the feed forward gain.

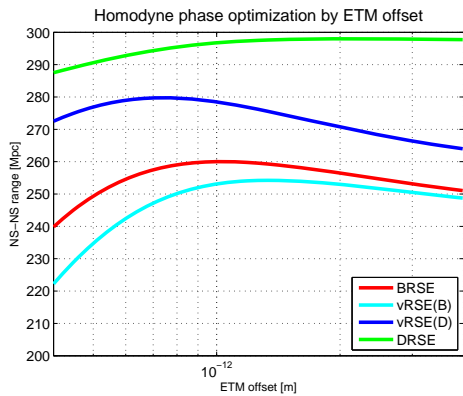


Figure 27: Optimization of the NS-NS binary range for offsets on the end mirrors differentially as a homodyne phase.

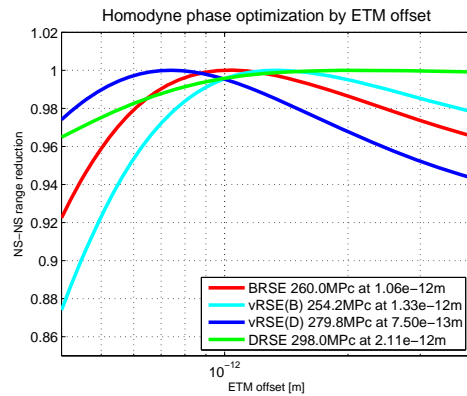


Figure 28: Dependence of the reduction of the NS-NS binary range on offsets on the end mirrors differentially as a homodyne phase.

interferometer. Therefore, it serves as the local oscillator for the sub-carrier, which is resonant in the dual-recycled Michelson, to sense the motion of SRM.

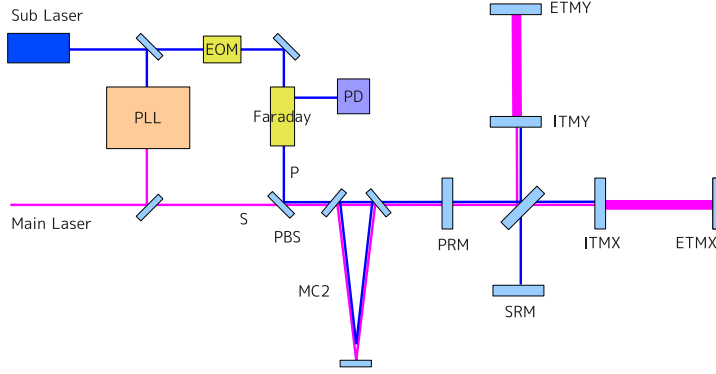


Figure 29: Conceptual setup of the sub-carrier injection scheme

For the sub-carrier to be resonant in the MC, its frequency offset from the main-carrier (f_{sc}) must be apart from the main carrier by $(n + 1/2)f_{MC}$, where n is an integer and f_{MC} is the FSR of the MC. This constraint gives us a set of discrete frequencies for possible f_{sc} . For each possible f_{sc} , we examined the detuning phase of the SRC to the main carrier when the sub-carrier is made resonant. We also checked the power build up of the sub-carrier inside the SRC. Figure 30 shows the result. We picked only the f_{sc} candidates with more than 4 times of power enhancement of the sub-carrier in the SRC and plotted them. The horizontal axis of the figure is the detuning phase of the SRC and the vertical axis is the power enhancement factor.

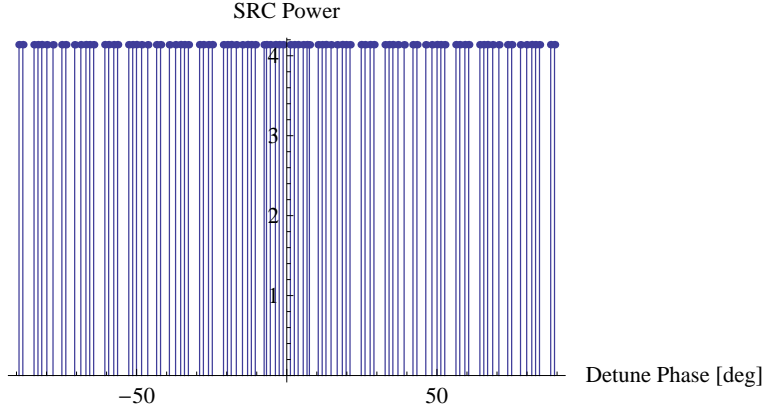


Figure 30: Scan of sub-carrier frequency.

As we can see from the figure, the detuning phase of the SRC can be chosen relatively freely by changing f_{sc} , although it is discrete. To make figure 30, we scanned f_{sc} for ± 1 GHz.

The PLL part of this scheme includes a double-pass AOM to shift the frequency of either the sub-carrier or the main-carrier. This is to make the beat frequency not too high (like 1 GHz). The error signal from the MC is fed back to the frequency of the AOM driver to resonate the sub-carrier in the MC. We will use wave front sensors (WFSs) to monitor the mis-alignment between the sub-carrier beam and the MC. The WFS signals will be fed back to the sub-carrier's steering mirrors to align the sub-carrier and the main-carrier beams.

References

- [1] Y. Levin, Phys. Rev. D **57**, 659 (1998)
- [2] G. Harry *et al*, Class. Quantum Grav. **19**, 897 (2002)
- [3] G. González, Class. Quantum Grav., **17**, 4409 (2000)
- [4] K. Yamamoto, Sec. 3, LCGT Design Document, internal report, (2004)
- [5] A. Buonanno and Y. Chen, Phys. Rev. D, **64**, 042006 (2001)
- [6] Advanced LIGO Conceptual Design Report, LIGO-T070247 (2008)
- [7] "LCGT Length Sensing and Control," K. Somiya, JGW-T0500048-v1, in Japanese (2005)
- [8] "Length Sensing and Control for AdLIGO," K. Somiya, O Miyakawa, P. Fritschel, and R. Adhikari, LIGO-DCC T060272 (2006)
- [9] "Measurement of optical response of a detuned resonant sideband extraction gravitational wave detector," O. Miyakawa *et al.*, Phys. Rev.D, **74**, 022001 (2006)
- [10] "Diagonalization of the length sensing matrix of a dual recycled laser interferometer gravitational wave antenna," S. Sato *et al.*, Phys. Rev.D, **75**, 082004 (2007)
- [11] "Experimental investigation of a control scheme for a zero-detuning resonant sideband extraction interferometer for next-generation gravitational-wave detectors," F. Kawazoe *et al.*, Class. Quantum Grav., **25**, 195008 (2008)
- [12] "Development of a signal-extraction scheme for resonant sideband extraction," K. Kokeyama *et al.*, Class. Quantum Grav., **25**, 235013 (2008)
- [13] V. Kalogera, ERRATUM:" THE COSMIC COALESCENCE RATES FOR DOUBLE NEUTRON STAR BINARIES ", ApJ, 601, L179 [2004])
- [14] V. Kalogera, et.al., "THE COSMIC COALESCENCE RATES FOR DOUBLE NEUTRON STAR BINARIES ", ApJ, 601:L179?L182, 2004
- [15] Kim, C., " Galactic Pulsar Population: Current Understanding and Future Prospects ", in Bassa, C.G., Wang, Z., Cumming, A., and Kaspi, V.M., eds., 40 Years of Pulsars: Millisecond Pulsars, Magnetars and More, McGill University, Montréal, Canada, 12-17 August 2007, AIP Conference Proceedings, vol. 983, pp. 576?583, (American Institute of Physics, Melville, U.S.A., 2008).
- [16] LivingRev. Relativity, 11, (2008), 8, <http://www.livingreviews.org/lrr-2008-8>
- [17] Phinney, E. S. 1991, ApJ, 380, L17
- [18] Kalogera, V., Narayan, R., Spergel, D. N., Taylor, J. H. 2001, ApJ, 556, 340
- [19] H.Tagoshi, <http://www.gw.hep.osaka-cu.ac.jp/GWAnote/023.note2.tagoshi.pdf>
- [20] N.Kanda, <http://www.gw.hep.osaka-cu.ac.jp/LCGT/WholeSky.pdf>
- [21] D.Tatsumi, http://gw.icrr.u-tokyo.ac.jp:8888/JGWwiki/LCGT/subgroup/analysis/gw_search?action=AttachFile&do=get&target=ns_event_estimation.pdf

- [22] E.E.Flanagan and S.A.Hughes, Phys.Rev.D **57**, 4535 (1998)
- [23] S. Ando et al. PRL 95, 171101 (2005)
- [24] Dimmelmeier, Ott, Marek and Janka, PRD 78, 064056 (2008)
- [25] N. Kanda and the TAMA Collaboration, Class. Quantum Grav., 20 (2003) S761